Experimental Investigation on Low-Velocity Impact Response and Residual Compressive Bearing Capacity of Composite Stringers

CHEN Fang, YAO Weixing, WU Fuqiang*

State Key Laboratory of Mechanics and Control of Mechanical Structures, Nanjing University of Aeronautics and Astronautics, Nanjing 210016, P. R. China

(Received 10 June 2020; revised 12 July 2020; accepted 30 July 2020)

Abstract: Three types of composite stringers were impacted from two different directions. Relationships between impact energy and visible defect length were found. The critical impact energy corresponding to barely visible impact damage (BVID) of each stringer was determined. Specimens with BVID were then compressed to obtain the residual strength. Experimental results showed that for all types of stringers, the critical energy of in-plane impact is always much lower than out-plane ones. In-plane impact causes much more decrement of stringers' bearing capacity than out-plane impact. For both impact directions, I-stringers own the highest defect detectability, T-stringers come second. Meanwhile, T-stringers own the better residual strength ratio than I-stringers and J-stringers. Synthetic considering impact defect detectability and residual bearing capacity after impact, T-stringers own the best compression-after-impact (CAI) behaviors.

Key words: composite stringer; low-velocity impact defect; compression after impact; residual bearing capacity

CLC number: V258 **Document code:** A **Article ID:** 1005-1120(2020)04-0655-08

0 Introduction

Nowadays, composite is no longer a new material it once was. Based on the various studies of composites' physical and mechanical properties, usage of composite structure has become as popular and important as metal structure does. However, just as composite owns some advantages that metal does not, composites' disadvantages also bring new challenges that people never meet during metal structure design. Composites' impact responses and their mechanical behaviors after impact are one of these challenges[1-2]. Advisory circular 20-107B made by the Federal Aviation Administration (FAA) indicated that the low detectable impact damage is very likely to cause obvious decrement of composite structures' load-bearing behaviors, especially the residual compression strength. Therefore, aviation composite structures' compression after impact (CAI) responses are needed urgently in research[3-5].

For decades, researchers have made some progress. Cantwell et al.[6] found the threshold energy for impact damage from their experiment results. Moura et al.[7] proposed that composites' delamination damage after impact only located at the interlaminar region of plies with different angles. Robinson et al.[8] studied the relationship between impact damage and composites' geometry parameters. Jia et al.[9] dealt with the impact damage initiation and propagation in cruciform laminated plates. Huan et al.[10] tested impact responses of carbon fiber reinforced polymer (CFRP) sandwich plates. Mishra et al.[11] and Esrail et al.[12] analytically studied the impact damage initiation and quantification of compos-

*Corresponding author, E-mail address: wxyao@nuaa.edu.cn.

How to cite this article: CHEN Fang, YAO Weixing, WU Fuqiang. Experimental investigation on low-velocity impact response and residual compressive bearing capacity of composite stringers[J]. Transactions of Nanjing University of Aeronautics and Astronautics, 2020, 37(4): 655-662.

http://dx.doi.org/10.16356/j.1005-1120.2020.04.016

ite laminates. Naik et al.[13] considered the effects of laminate configuration on composite plates' impact responses.

Apart from the investigation of out-plane central-point impact responses of singular laminated plate, researchers also became interested in other topics, such as in-plane edge impact and CAI behaviors of composite structures. Ostre et al.[14-15] conducted experiments to study the in-plane impact and proposed a corresponding simulation method. Malhotra et al.[16] compared the difference between in-plane impact and near-edge impact. Abir et al.[17] investigated the relationship between failure mechanism and residual compression strength of composites. Caprino[18] and Nyman et al.[19] proposed an equivalent impact damage method to predict residual strength for composite structures. Li et al.[20], Sun et al.[21] and Feng et al.[22] investigated composite stiffened panels' impact response and their residual strength. Greenhalgh et al.[23-24] investigated the influences of different impact defects on the compressive responses of CFRP stringer-stiffened panels. Ishikawa et al.[25] tried to find the temperature effects on stiffened panels' CAI behaviors. However, the problems on composite structures' impact damage and CAI responses caused by out-plane and in-plane edge impact still need to be further studied.

Therefore, the aim is to experimentally investigate the laminated stringers' impact damage and CAI behaviors under different cross-sectional types and impact directions. In this paper, three different types of laminated composite stringers' CAI behaviors were tested. Two kinds of edge-impact load (both in-plane impact and out-plane impact) were separately applied to six specimen groups. Stringers' impact responses were obtained and the certain energy level corresponding to barely visible impact damage (BVID) was discussed. Six groups' stringers with a same visible defect length were compressed to obtain residual compressive strength. Impact damage visible detectability and residual bearing capacity were set as indicators for judging laminated composite stringers' CAI behaviors.

1 Experiment

1.1 Specimen

Specimens are 200 mm-long composite stringers with two ends embedded into polymer foam (Fig.1). Stringers are divided into three groups according to different cross section types (i.e., I-stringer, J-stringer and T-stringer). Their cross-section shape and dimension parameters are shown in Fig.1. Three kinds of stringers have same cross-section area and weight.

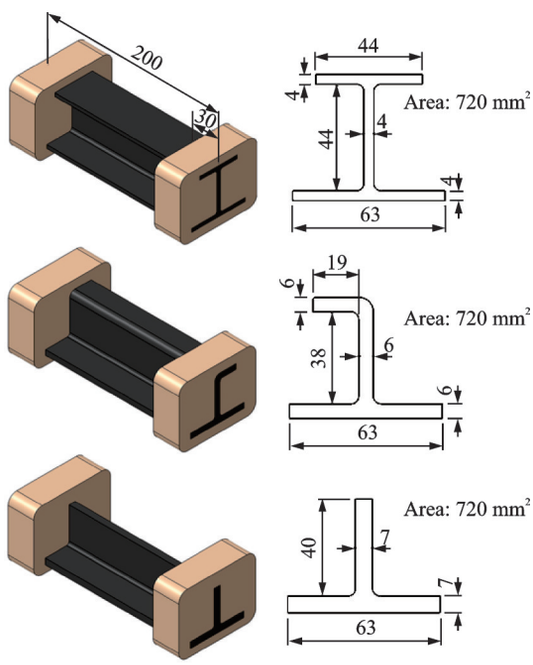

Fig.1 Geometric construction of stringers (Unit: mm)

All specimens were laminated by carbon-fiber/epoxy resin prepreg with thickness of 0.184 mm. And the corresponding stacking sequence was $[\pm 45/0_3/45/0_2/-45/90/45/0]_S$ for I-stringer, $[\pm 45/0_2/45/0_2/-45/0_2/45/90_2/-45/0]_S$ for J-stringer and $[\pm 45/0_2/45/0_2/-45/0_2/45/0_2/-45/90_2/45/0]_S$ for T-stringer. Specimens were named as SEDN (e.g., TVI1), where S represents cross-section type (i.e., I for I-stringer, J for J-stringer and T for T-stringer), E represents impact energy category (i.e., V for variable impact energy or C for constant impact energy), D represents impact direction (i.e., I for in-plane impact or O for out-plane impact) and N represents serial number. For example, JCO2 represents the second J-stringer which is

impacted under constant out-plane impact energy.

1.2 Experiment method

Before formal test, each specimen was named and visual checked. Specimens with initial defect were picked out of experimental groups. For each group, at least 12 specimens were impacted from two directions (Fig.2). Six of them were in-plane impacted and other six were out-plane impacted. They were all impacted under different impact energy to find energy-defect relationships. After they were impacted, the defect length would be measured immediately. This measurement should be conducted with the same measure instrument and under the same atmosphere (i.e., A same researcher used same measure tools and maintained a same posture under a same illumination condition). If energy-defect relationship was difficult to generalize, more specimens would be impacted.

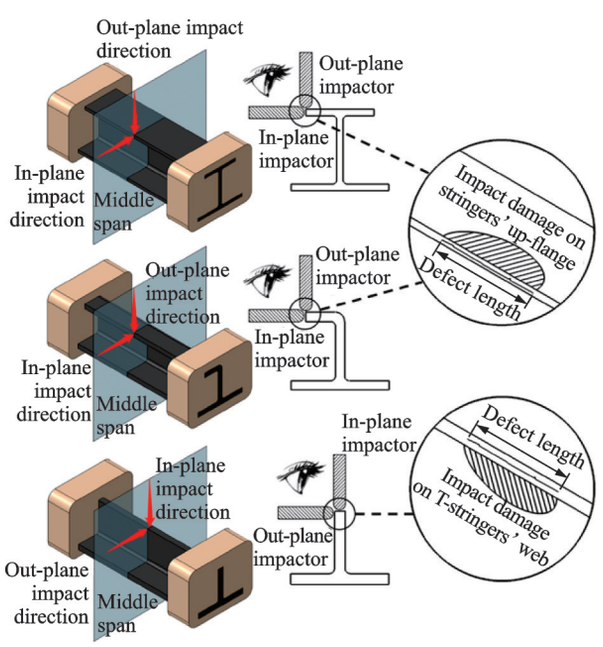

Fig.2 Impact direction and defect length measurement of stringers

The impact energy that leads BVID is defined as critical impact energy (CIE) in this paper. Based on energy-defect relationships and BVID value, in-plane and out-plane CIE values of three groups can be found. For each group, three more specimens were in-plane or out-plane impacted under the corresponding CIE. After that, these specimens were uniaxial compressed to obtain damage distribution and residual strength.

1.3 Experiment equipment

Impact experiments were conducted on drop hammer testing machine MTS ZCJ9162, which met the main test device requirements mentioned in standard ASTM-D3716. Its steel impactor was 16 mm in diameter and the maximum impact energy it could generate was 160 J. After the impactor was rebounded, a rubber chuck would stop the impactor in order to avoid producing unexpected additional impact damage. Uniaxial compression after impact was conducted on MTS 370 servohydraulic test system, which can meet the test device requirements mentioned in standard ASTM-7137.

2 Results

2.1 Energy-defect relationship curve

Thirty-six stringers were averagely divided into six groups according to different impact directions and cross-section shapes. Specimens within each group were impacted under variable kinetic energy to obtain relationships between defect length and impact energy. Test results of certain groups did not show data variation tendency clearly, so 13 more specimens were additionally impacted. All these 49 stringers' impact test data and the logarithm-fitting curves are shown in Figs.3—5.

In Figs.3—5, no matter what the stringers' section type is, in-plane impact test data always locate in the left side of out-plane test results. Moreover, within each groups' scattering plot of visible defect v.s. impact damage, a soft data-inflection can

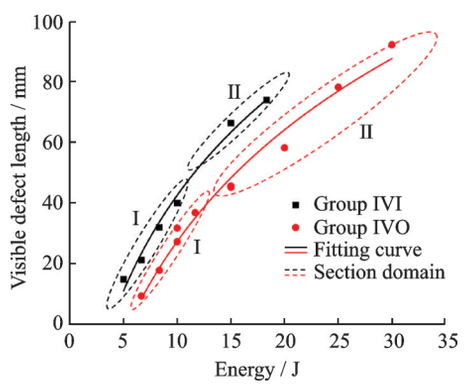

Fig.3 I-stringer impact test data and energy-defect curve

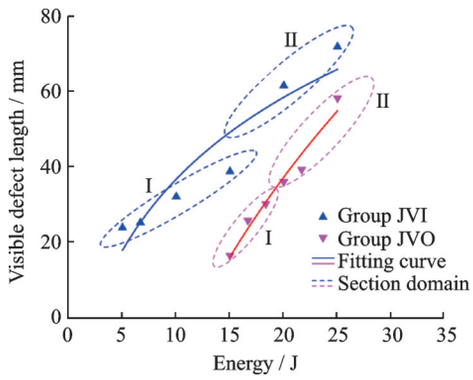

Fig.4 J-stringer impact test data and energy-defect curve

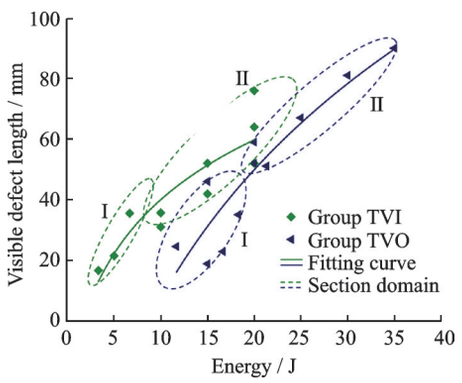

Fig.5 T-stringer impact test data and energy-defect curve

be found and two data sections are divided according to different variation rate. For almost all groups, except group JVI, the data variation rate of Section I is higher than that of Section II. This characteristic also demonstrates that logarithm function is a good choice for the fitting curve.

2.2 Critical impact energy

FAA defined BVID as the impact damage at the threshold of reliable detection when using a visual inspection procedure. In present work, the dimension of BVID is set as 30 mm according to the reference value given by aircraft tolerance design manual. And the intersection point of BVID dimension with defect-energy curves is defined as critical impact energy E_{cr}. On the basis of this definition and 30 mm BVID length, each groups' critical impact energy is determined (Fig.6).

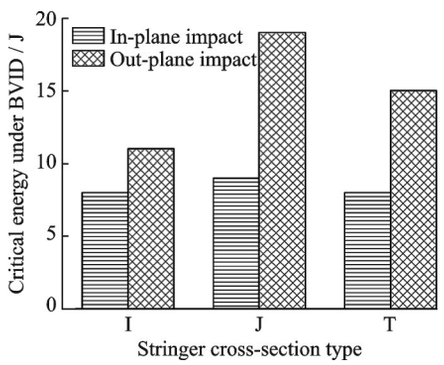

Fig.6 Stringers' critical impact energy

For all three cross-section types investigated in this paper, in-plane impact events own higher E_{cr} than out-plane ones. To verify the accuracy of results shown in Fig.6, 18 more stringers of six groups were impacted under the corresponding critical impact energy. These constant-energy impact test results were statistically shown in Table 1, where all the average visible defect lengths of six groups approximate to 30 mm (i.e., the predefined BVID dimension). This can enhance the reliability of Fig.6, and verify the effectiveness of energy-defect fitting curves obtained in Section 2.1.

2.3 Residual bearing capacity

Eighteen stringers of six groups, listed in the first column in Table 1, were uniaxially compressed after impact. Fig.7 shows their residual bearing capability F_{rbc}, which is compared with the reference value F_{ibc} (i.e., initial bearing capacity obtained by compressing intact stringers without impact defect). Eq.(1) is used to calculate the absolute decrement of bearing load R_{bc} (Table 2). Stringers of group ICO were impacted under higher energy-level, how-

Table 1 Impact results under constant energy of stringers

Group name	Impact direction	Impact defect / mm	Average defect / mm
ICI1—ICI3	In-plane	37.5, 32.0, 29.5	33.0
ICO1—ICO3	Out-plane	19.8, 24.9, 33.8	26.2
JCI1—JCI3	In-plane	27.9, 26.9, 32.3	29.0
JCO1—JCO3	Out-plane	28.7, 24.2, 35.7	29.5
TCI1—TCI3	In-plane	30.7, 29.7, 42.4	34.3
TCO1—TCO3	Out-plane	11.0, 36.6, 37.8	28.5

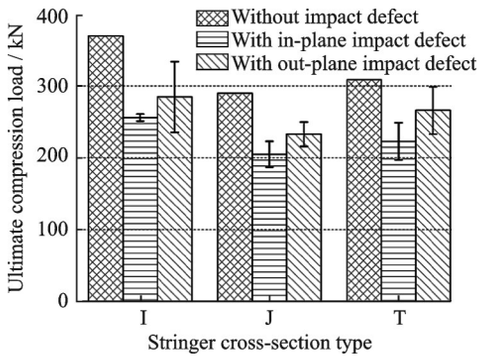

Fig.7 Stringers' CAI test results

Table 2 Decrement of bearing capacity of stringers

Group	ICI	ICO	JCI	JCO	TCI	TCO
R_{bc} / kN	114	85	85	57	85	43
Average	100		71		64	

ever, group ICI owned much more decrement of stringers' bearing capacity. Moreover, same results are also observed for J-stringers and T-stringers.

$$R_{bc} = F_{ibc} - F_{rbc} \tag{1}$$

2.4 Compression fracture modes

At the mesoscopic level, 18 stringers' final fracture is all resulted from the combination with matrix crack, fiber/matrix debonding, delamination and fiber failure. At the macroscopic scale, impact-point fracture (Fig.8(a)) and potting-end fracture (Fig.8(c)) are two main fracture modes within all stringers. The special one is JCO1, where both fracture modes are found (Fig.8(b)). All stringers' compression failure modes are statistically recorded in Fig.8(d). After in-plane impact, all cross-section types of stringers' break at the impact point. However, after out-plane impact, only 67% of I-stringers and 75% J-stringers break at impact point. Furthermore, all T-stringers' are found in potting-end fracture modes.

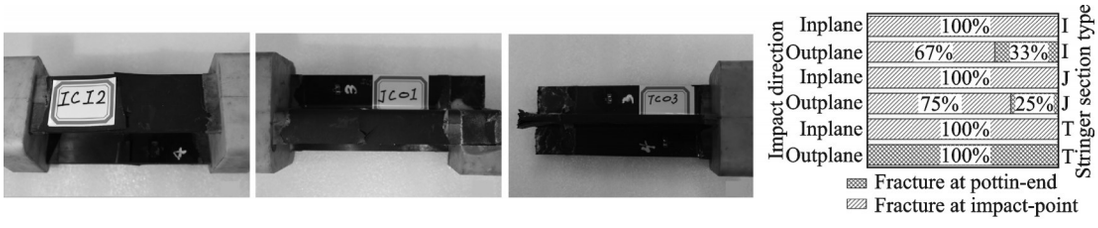

(a) Impact-point fracture (b) Mixed fracture (c) Potting-end fracture (d) Statistical data of fracture modes

Fig.8 Stringers' fracture modes of CAI tests

Both the alteration of material properties near impact point and the geometric shape changing at potting-end can cause stress concentration. And the mesoscale failure evolution induced by stress concentration results in whole structures' fracture. Theoretically speaking, stringers with impact defect are more likely to fracture at impact point, for the stress intensification caused by impact load is usually severe. Only undamaged or low-damaged stringers will fracture at potting-end. In other words, stringers with potting-end fracture mode own lower impact defect and higher residual bearing capacity than those with impact-point mode (Table 2 and Fig.8).

3 Discussion

Here, we define an indicator I_{idd} that can reflex the severity of impact events' low-detectability, which is the primary threat to structures' serviceability safety. Defect detectability depends on the detection sensitivity of inspection procedure. I_{idd} of certain stringers can be defined by each points of defect-damage curves via their horizontal and vertical coordinates

$$I_{idd} = \frac{E}{D} \tag{2}$$

where E and D represent impact defect length and impact energy threshold, respectively. Obviously, the longer the defect length, the less the undetected. From a statistical point of view, higher energy threshold means more impact events with lower impact energy become undetectable.

E_{th} and E_{cr} are two special points because they are the interfaces among three stages of defect v.s. energy curves. The first one is invisible stage, and the other two are visible stages with high increasing rate and low processing rate(i.e., Sections I and II

in Figs.3—5). The interface between visible and invisible stages, as well as the intersection point of defect v.s. energy curves with positive X-axis, is usually defined as energy threshold E_{th}. Moreover , the interface between two visible stages is a data domain ranging from 30 mm to 50 mm in the defect length. Its lower boundary just approximates stringers' D_{bvid} dimension, where the corresponding energy is E_{cr}. However, the measurement of E_{th} is difficult and uncertain because it is hard to find a material state with absolute zero defect length. Therefore, E_{cr} with D_{bvid} is substituted into Eq.(2) , and the new indicator for impact defect visible detectability is noted as I_{idvd}.

$$I_{idvd} = \frac{E_{cr}}{D_{bvid}} \tag{3}$$

where E_{cr} and D_{bvid} represent impact defect length and impact energy threshold, respectively. Table 3 shows six groups' calculation results of Eq.(3). As mentioned above, I_{idvd} represents the severity of undetectable for impact defects. In other words, the lower the I_{idvd}, the higher the defect visible detectability.

Table 3 Visible defect detectability of stringers

Group	ICI	ICO	JCI	JCO	TCI	TCO
I_{idvd} / N	242	420	310	644	233	526
Average	331		477		380	

From the aforementioned test results and discussion, within all three types of stringers, in-plane impact always results in defects with high defect visible detectability and low residual bearing capacity. In addition, judging from mechanical responses, in-plane impact is more dangerous than out-plane one because in-plane impact leads to the bigger defect and lower residual strength. Furthermore, judging from defect detectability, stringers' impact with in-plane load will be easier detected and repaired more timely. Another comparison result is also valuable: Despite of little difference among stringers' stacking sequence, T-stringers own relative higher defect visible detectability and cause the lowest decrement on bearing capacity.

4 Conclusions

Laminated composite stringers with three kinds of cross-sectional type were impacted and their CAI behaviors were also experimentally investigated. Several conclusions can be drawn.

(1) Logarithm functions can describe the defect-energy curves well, which owns two visible stages with different defects' increasing rates.

(2) In-plane impact brings a severe negative influence on stringers' residual bearing capacity, and impact defects caused by out-plane impact are difficult to be visibly detected.

(3) Synthetically evaluated from defect visible detectability and residual bearing capacity, T-stringer is the best choice among the three sectional types of stringers with similar stacking sequences.

References

[1] PHAM D C, LUA J, SUN H T, et al. A three-dimensional progressive damage model for drop-weight impact and compression after impact[J]. Journal of Composite Materials, 2020, 54(4): 449-462.

[2] SASIKUMAR A, TRIAS D, COSTA J, et al. Impact and compression after impact response in thin laminates of spread-tow woven and non-crimp fabrics[J]. Composite Structures, 2019, 215(1): 432-445.

[3] TUO H L, LU Z X, MA X P, et al. Damage and failure mechanism of thin composite laminates under low-velocity impact and compression-after-impact loading conditions[J]. Composites Part B—Engineering, 2019, 163(1): 642-654.

[4] THORSSON S I, SRINGERI S P, WAAS A M, et al. Experimental investigation of composite laminates subject to low-velocity edge-on impact and compression after impact[J]. Composite Structures, 2018, 186(1): 335-346.

[5] LIV Y, GUILLAMET G, COSTA J, et al. Experimental study into compression after impact strength of laminates with conventional and nonconventional ply orientations[J]. Composites Part B—Engineering, 2017, 126(1): 133-142.

[6] CANTWELL W J, MORTON J. Geometrical effects in the low velocity impact response of CFRP[J]. Composite Structures, 1989, 12(1): 39-59.

[7] MOURA D M, MARQUES A T. Prediction of low velocity impact damage in carbon-epoxy laminates[J]. Composites Part A—Applied Science and Manufactur-

ing, 2002, 33(3): 361-368.

[8] ROBINSON P, DAVIES G. Impactor mass and specimen geometry effects in low velocity impact of laminated composites[J]. International Journal of Impact Engineering, 1992, 12(2): 189-207.

[9] JIA W B, WEN W D, FANG L. Damage initiation and propagation in composites subjected to low-velocity impact: Experimental results, 3D dynamic damage model, and FEM simulations[J]. Transactions of Nanjing University of Aeronautics and Astronautics, 2019, 36(3): 488-499.

[10] HUAN D J, DING B, LI Y, et al. High velocity impact experiment on Ti/CFRP/Ti sandwich structure[J]. Transactions of Nanjing University of Aeronautics and Astronautics, 2015, 32(1): 121-127.

[11] MISHRA A, NAIK N K. Failure initiation in composite structures under low-velocity impact: Analytical studies[J]. Composite Structures, 2010, 92(1): 436-444.

[12] ESRAIL F, KASSAPOGLOU C. An efficient approach for damage quantification in quasi-isotropic composite laminates under low speed impact[J]. Composites Part B—Engineering, 2014, 61(1): 116-126.

[13] NAIK N K, MEDURI S. Polymer matrix composites subjected to low-velocity impact: Effect of laminate configuration[J]. Composite Science and Technology, 2001, 61(1): 1429-1436.

[14] OSTRE B, BOUVET C, LACHAUD F, et al. Edge impact damage scenario on stiffened composite structure[J]. Journal of Composite Materials, 2015, 49(13): 1599-1612.

[15] OSTRE B, BOUVET C, MINOT C, et al. Experimental analysis of CFRP laminates subjected to compression after edge impact[J]. Composite Structures, 2016, 152(1): 767-778.

[16] MALHOTRA A, GUILD F J, PAVIER M J. Edge impact to composite laminates: Experiments and simulations[J]. Journal of Materials Science, 2008, 43(20): 6661-6667.

[17] ABIR M R, TAY T E, RIDHA M, et al. On the relationship between failure mechanism and compression after impact strength in composites[J]. Composite Structures, 2017, 182(1): 242-250.

[18] CAPRINO G. Residual strength prediction of impacted CFRP laminates[J]. Journal of Composite Materials, 1984, 18(6): 508-518.

[19] NYMAN T, BREDBERG A, SCHON J. Equivalent damage and residual strength for impact damaged composite structures[J]. Journal of Reinforced Plastics and Composites, 2000, 19(6): 428-448.

[20] LI N, CHEN P H. Experimental investigation on edge impact damage and compression-after-impact (CAI) behavior of stiffened composite panels[J]. Composite Structures, 2016, 138(1): 134-150.

[21] SUN W, GUAN Z, OUYANG T, et al. Effect of stiffener damage caused by low velocity impact on compressive buckling and failure modes of T-stiffened composite panels[J]. Composite Structures, 2018, 184(1): 198-210.

[22] FENG Y, ZHANG H, TAN X, et al. Effect of impact damage positions on the buckling and post-buckling behaviors of stiffened composite panel[J]. Composite Structures, 2016, 155(1): 184-196.

[23] GREENHALGH E, BISHOP S M, BRAY D, et al. Characterization of impact damage in skin-stringer composite structures[J]. Composite Structures, 1996, 36(3): 187-207.

[24] GREENHALGH E, MEEKS C, CLARKE A, et al. The effect of defects on the performance of post-buckled CFRP stringer-stiffened panels[J]. Composites Part A, 2003, 34(7): 623-633.

[25] ISHIKAWA T, MATSUSHIMA M, HAYASHI Y, et al. Experiments and numerical analysis of compression after impact (CAI) behavior of CF/PIXA stiffened panels for HSCT structure[J]. Advanced Composite Materials, 2005, 14(3): 239-261.

Acknowledgements This work was supported in part by the National Key Basic Research and Development Plan ("973" Plan) (No. 613274) and the Priority Academic Program Development of Jiangsu Higher Education Institutions (PAPD).

Authors Dr. **CHEN Fang** received the B.S. degree in aircraft design and engineering from Nanjing University of Aeronautics and Astronautics (NUAA) in 2013. He is currently a doctoral candidate majoring in aircraft design of NUAA. His research domain is the progressive damage simulation analysis of composite structures.

Prof. **YAO Weixing** is a Ph.D. tutor in Aerospace College of NUAA. His research interests are composite materials damage mechanics, aircraft multidisciplinary design, and struc-

tural fatigue analysis. He has published more than 200 academic papers on well-known domestic and foreign journals, as well as four widely-used monographs. He has also won five technology progress awards.

Author contributions Prof. **YAO Weixing** designed the whole study. Dr. **CHEN Fang** and Dr. **WU Fuqiang** contributed the experimental data. Dr. **CHEN Fang** also complied the analysis, investigated the results and wrote the manuscript. All authors commented on the manuscript draft and approved the submission.

Competing interests The authors declare no competing interests.

(Production Editor: ZHANG Tong)

复合材料长桁结构低速冲击响应及剩余压缩承载能力的试验研究

陈 方，姚卫星，吴富强

(南京航空航天大学机械结构力学及控制国家重点实验室，南京 210016，中国)

摘要：对3种截面形状的复合材料长桁实施了2类冲击方向的损伤试验，建立了冲击能量与可见损伤尺度之间的内在联系，并据此确定了3种复合材料长桁产生勉强目视可见冲击损伤(Barely visible impact damage, BVID)所需的临界冲击能量。针对含有BVID的复合材料长桁试样，进行了额外的冲击后压缩试验，测得每种复合材料长桁的剩余压缩强度。研究结果表明，3种不同截面形状的复合材料长桁均呈现一致的规律：相对于面外冲击载荷，面内冲击载荷对应着更小的临界冲击能量以及更大的剩余强度衰减幅度。研究还表明在2种不同方向的冲击载荷影响下，I型长桁具有最高的冲击损伤可见度、且T型长桁居中、J型长桁最弱。同时，T型长桁具有最高的剩余承载能力、且J型长桁居中、I型长桁最弱。综合冲击损伤可见度及剩余承载能力2个关键指标，可认为3种截面形状中，T型复合材料长桁性能最优。

关键词：复合材料长桁；低速冲击损伤；冲击后压缩；剩余承载能力